EUROPEAN ORGANIZATION FOR NUCLEAR RESEARCH

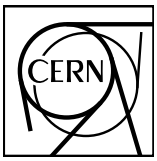

CERN-EP-2023-020
17 February 2023

Measurement of the Λ hyperon lifetime

ALICE Collaboration

Abstract

A new, more precise measurement of the Λ hyperon lifetime is performed using a large data sample of Pb–Pb collisions at $\sqrt{s_{\rm NN}} = 5.02$ TeV with ALICE. The Λ and $\overline{\Lambda}$ hyperons are reconstructed at midrapidity using their two-body weak decay channel $\Lambda \to {\rm p} + \pi^-$ and $\overline{\Lambda} \to \overline{\rm p} + \pi^+$. The measured value of the Λ lifetime is $\tau_{\Lambda} = [261.07 \pm 0.37\ ({\rm stat.}) \pm 0.72\ ({\rm syst.})]$ ps. The relative difference between the lifetime of Λ and $\overline{\Lambda}$, which represents an important test of CPT invariance in the strangeness sector, is also measured. The obtained value $(\tau_{\Lambda} - \tau_{\overline{\Lambda}})/\tau_{\Lambda} = 0.0013 \pm 0.0028\ ({\rm stat.}) \pm 0.0021\ ({\rm syst.})$ is consistent with zero within the uncertainties. Both measurements of the Λ hyperon lifetime and of the relative difference between τ_{Λ} and $\tau_{\overline{\Lambda}}$ are in agreement with the corresponding world averages of the Particle Data Group and about a factor of three more precise.

1 Introduction

The Λ is the lightest hyperon, with strangeness $S = -1$, isospin $I = 0$, and quark content uds. Its lifetime has been measured in past experiments starting from 1963 using its weak decay channels $\Lambda \to \mathrm{p} + \pi^-$ and $\overline{\Lambda} \to \overline{\mathrm{p}} + \pi^+$. The world average reported in the Review of Particle Physics of the Particle Data Group (PDG) [1] is $\tau_\Lambda = 263.2 \pm 2.0$ ps. This is the result of averaging the measurements performed in 1973 by Poulard et al. [2] and 1975 by Clayton et al. [3] using Λ produced in interactions of low-energy charged kaon beams with a fixed target, and the measurement of Zech et al. [4] in 1977 using a neutral hyperon beam. These results are based on data samples containing a maximum of fifty-three thousand events. The relative difference between the lifetimes of Λ and $\overline{\Lambda}$ reported in the PDG is $(\tau_\Lambda - \tau_{\overline{\Lambda}})/\tau_\Lambda = -0.001 \pm 0.009$, resulting from the average of two measurements, one performed in 1967 by Badier et al. [5] and another one in 1996 by Barnes et al. [6], using Λ and $\overline{\Lambda}$ produced in low-energy $\mathrm{p} + \overline{\mathrm{p}} \to \Lambda + \overline{\Lambda}$ reactions. The excellent tracking and particle-identification capabilities of ALICE over a broad momentum range and the large amount of data collected during Run 2 of the LHC are exploited to improve the current precision on the measurement of the Λ lifetime and on the relative difference between the lifetimes of Λ and $\overline{\Lambda}$. The latter provides a fundamental test of CPT invariance in the strangeness sector.

This measurement is also a fundamental reference for the studies of the properties of hypernuclear states created in heavy-ion collisions and for future precision studies of other hyperon properties. The analysis presented here is performed in Pb–Pb collisions at a center-of-mass energy $\sqrt{s_{\mathrm{NN}}} = 5.02$ TeV using the same data sample employed for the measurements of the (anti)hypertriton lifetime and Λ separation energy [7]. The latter measurements are fundamental to infer the internal structure of this hypernucleus as well as the properties of hyperon–nucleon interaction in the low-density limit, as described in [8].

2 Experimental apparatus

ALICE is one of the four large experiments at the LHC and it is dedicated to the study of heavy-ion collisions at ultrarelativistic energies. A detailed description of the ALICE apparatus and its performance can be found in Refs. [9] and [10]. In the following, only the subdetector systems used for the analysis presented in this paper are described.

Trajectories of charged particles are reconstructed in the ALICE central barrel with the Inner Tracking System (ITS) [11] and the Time Projection Chamber (TPC) [12]. These are located within a large solenoidal magnet, providing a highly homogeneous magnetic field of 0.5 T parallel to the beam axis. The ITS consists of six cylindrical layers of silicon detectors, concentric and coaxial to the beam pipe, with a total pseudorapidity coverage $|\eta| < 0.9$ with respect to the nominal interaction point. Three different technologies are used for this detector: the two innermost layers consist of silicon pixel detectors (SPD), the two central layers of silicon drift detectors (SDD), and the two outermost layers of double-sided silicon strip detectors (SSD). This detector is used in the determination of primary and secondary vertices, and in the track reconstruction.

The TPC is the largest detector in the ALICE central barrel, with a pseudorapidity coverage $|\eta| < 0.9$. It is used for charged-particle track reconstruction, momentum measurement, and particle identification (PID) via the measurement of the specific energy loss ($\mathrm{d}E/\mathrm{d}x$) of particles in the TPC gas. This detector provides up to 159 spacial points per track for charged-particle reconstruction. The resolution in the measurement of the distance-of-closest approach of primary tracks to the primary collision vertex, projected on the transverse plane, ranges from about 200 μm at 0.2 GeV/c to about 10 μm at 10 GeV/c [10]. The transverse-momentum (p_{T}) resolution ranges from about 1% at 1 GeV/c to about 10% at 50 GeV/c in Pb–Pb collisions at $\sqrt{s_{\mathrm{NN}}} = 5.02$ TeV [13]. The $\mathrm{d}E/\mathrm{d}x$ resolution depends on the event multiplicity and is about 5–6.5% for minimum-ionizing particles crossing the full volume of the TPC [10].

The PID is complemented by the Time-Of-Flight (TOF) system [14]. This detector is made of Multi-

gap Resistive Plate Chambers (MRPC) and is located at a radial distance of 3.7 m from the nominal interaction point. The TOF detector measures the arrival time of particles relative to the event collision time provided by the TOF detector itself or by the T0 detectors, two arrays of Cherenkov counters located at forward and backward rapidities [15]. The TOF detector is used in this analysis for pile-up rejection, mostly from out-of-bunch collisions, by requiring that at least one of the Λ ($\overline{\Lambda}$) charged decay-daughter tracks has an associated hit in the TOF detector.

Collision events are triggered by two plastic scintillator arrays, V0A and V0C [16], located on both sides of the interaction point, covering the pseudorapidity regions $2.8 < \eta < 5.1$ and $-3.7 < \eta < -1.7$, respectively. Each array consists of four concentric rings, each ring comprising eight cells with the same azimuthal coverage. The V0A and V0C scintillators are used to determine the collision centrality from the measured signals produced by charged particles [17, 18]. The centrality is defined in terms of percentiles of the total hadronic cross section.

3 Data analysis

3.1 Event selection

The data used for this analysis were collected in 2018 during the LHC Pb–Pb run at $\sqrt{s_{\rm NN}} = 5.02$ TeV. A minimum bias (MB) event trigger and two centrality triggers were used. The MB trigger, fully efficient in the centrality interval 0–90%, requires coincident signals in the V0 detectors, synchronous with the bunch crossing time defined by the LHC clock. The two centrality triggers, fully efficient in the centrality classes 0–10% and 30–50%, are based on the signal amplitude measured by the V0 scintillators, which is proportional to the charged-particle multiplicity of the event. The analysis is performed in four centrality classes: 0–10%, 10–30%, 30–50%, and 50–90%. The events in the centrality classes 0–10% and 30–50% are selected using both the MB and centrality triggers, while the MB event trigger alone is used for the other centrality classes. In order to keep the conditions of the detectors as uniform as possible and reject background collisions, the coordinate of the primary vertex along the beam axis is required to be within 10 cm from the nominal interaction point. Events with multiple vertices identified with the SPD are tagged as pile-up and removed from the analysis [10]. In addition, events with pile-up occurring during the drift time of the TPC are rejected based on the correlation between the number of SDD and SSD clusters and the total number of clusters in the TPC, as described in Ref. [19]. To further suppress the pile-up contribution, mostly from out-of-bunch collisions, the Λ daughter tracks are required to have an associated hit in the TOF detector. This requirement is applied only for the centrality classes 30–50% and 50–90%. For the most central events, the matching of daughter tracks with a TOF hit does not have a significant impact on the fraction of Λ ($\overline{\Lambda}$) from events with out-of-bunch pile-up, which is found to be between 0.02% and 0.07%. The total number of events selected for each centrality class is reported in Table 1.

Table 1: Number of events used for the analysis.

Centrality	Number of events ($\times 10^6$)
0–10%	70.97
10–30%	18.43
30–50%	61.43
50–90%	36.86

3.2 Selection of Λ candidates

The two-body decay channels $\Lambda \to \mathrm{p} + \pi^-$ and $\overline{\Lambda} \to \overline{\mathrm{p}} + \pi^+$ are used in this measurement. These have a branching ratio BR of $(63.9 \pm 0.5)\%$ [1]. The Λ ($\overline{\Lambda}$) candidates are reconstructed using the standard AL-

ICE weak decay finder. This algorithm searches for weak decay topologies, called V^0, by reconstructing oppositely-charged particle tracks originating from a displaced vertex as described in Refs. [20, 21]. In the case of a decay vertex located inside the ITS volume, at least one hit in any of the ITS layers is used in the reconstruction of the charged tracks originating from the V^0 decay. The reconstructed tracks, selected in the pseudorapidity region $|\eta| < 0.8$, are required to fulfil a set of quality criteria such as having a number of TPC crossed rows larger than 80, a number of TPC clusters used for the dE/dx calculation larger than 60 to ensure a good dE/dx resolution, a fraction of TPC crossed rows and findable clusters larger than 70%, and a good track fit $\chi^2/N_{\rm cls}^{\rm TPC} < 2.5$, where $N_{\rm cls}^{\rm TPC}$ is the number of TPC clusters.

To reduce the combinatorial background, a set of topological selections are applied, i.e. the distance of closest approach (DCA) between the V^0 daughter tracks is required to be less than 1 cm, the DCA between the V^0 and the primary collision vertex less than 0.5 cm, the radial distance between primary and secondary vertices larger than 3 cm, and $\cos(\theta_{\rm p}) > 0.995$, where $\theta_{\rm p}$ is the angle between the vector connecting the primary and secondary vertices and the total V^0 momentum ($\vec{p}_{\rm V^0} = \vec{p}_{\rm p} + \vec{p}_{\pi}$). The selection criteria applied for this measurement are similar to those already used in previous measurements [21–23].

The particle identification is based on the energy loss per unit of track length measured by the TPC. Protons and pions are identified by requiring that their measured dE/dx is within $3\sigma_{dE/dx}$ from the expected average calculated using the Bethe–Bloch, where $\sigma_{dE/dx}$ is the dE/dx resolution. Proton and pion candidates are selected in the transverse-momentum intervals $0.2 < p_{\rm T}^{\pi} < 2$ GeV/c and $0.2 < p_{\rm T}^{\rm p} < 10$ GeV/c, respectively.

3.3 Signal extraction

The Λ and $\overline{\Lambda}$ lifetimes are extracted from a fit to their proper decay length distributions using the exponential function $\exp\left(-L_{\rm proper}/\langle L_{\rm proper}\rangle\right)$. The proper decay length is calculated for every Λ ($\overline{\Lambda}$) as

$$L_{\rm proper} = L_{\rm lab}/\beta\gamma = M_{\Lambda}\frac{L_{\rm lab}}{p}, \tag{1}$$

where $L_{\rm lab}$ is the decay length measured in the laboratory system as the distance between primary and secondary vertices, M_{Λ} is the Λ mass taken from the PDG ($M_{\Lambda} = 1115.683$ MeV/c^2) [1], and p is the total momentum of the Λ ($\overline{\Lambda}$) measured at the decay point. The number of signal counts in each $L_{\rm proper}$ interval is obtained using the following procedure, which is illustrated in Fig. 1:

1. **Location of the peak region**: the invariant mass of the decay daughters is calculated and the region around the maximum of the invariant-mass distribution is fitted using a Gaussian function. The peak region is defined as $[M_0 - 8\sigma, M_0 + 10\sigma]$, where M_0 is the mean and σ is the standard deviation of the Gaussian fit. The choice of such a wide signal region is motivated by the fact that the peak has two long tails and is slightly asymmetric, especially for low values of $L_{\rm proper}$. This asymmetry is an effect of residual imperfections in tracking and energy loss corrections, which affect candidates with invariant masses above and below the expected mass differently.

2. **Fit of the background**: the background on the side bands of the peak is fitted using a continuous function to extrapolate the expected background inside the peak region. Since the background shape changes with $L_{\rm proper}$, a third-order polynomial function is used to fit the background at low $L_{\rm proper}$ while the sum of a power-law and a linear function is used at high $L_{\rm proper}$ values. These functions have the minimum number of parameters that guarantees a data-to-fit ratio consistent with unity within statistical uncertainties in the sidebands.

3. **Signal extraction**: the signal is extracted in each $L_{\rm proper}$ interval by subtracting the estimated background from the invariant mass distribution and counting the entries inside the peak region.

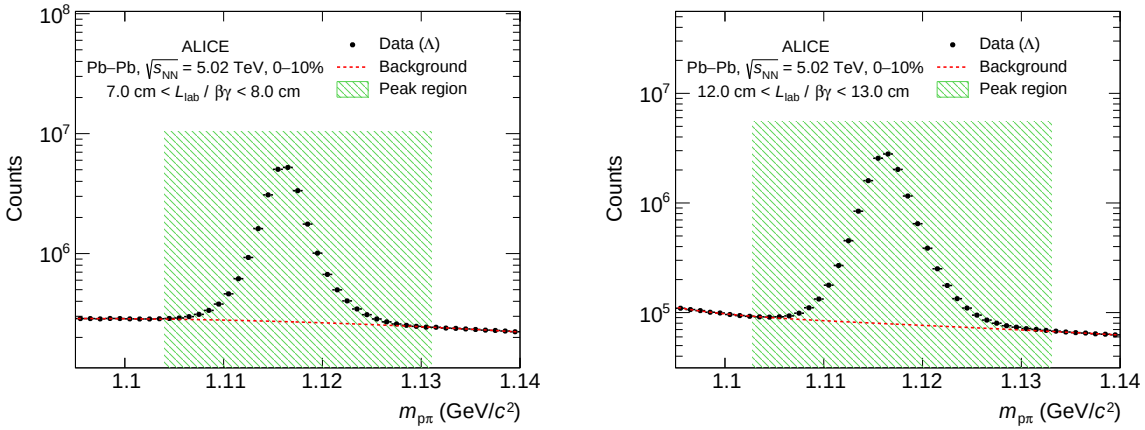

Figure 1: Invariant mass spectra of pπ pairs measured in central collisions (0–10%) at low (left) and large (right) L_{proper}. The green area indicates the peak region.

The total number of Λ and $\overline{\Lambda}$ raw counts within the peak region are reported in Table 2 for each centrality interval.

Table 2: Raw counts of Λ and $\overline{\Lambda}$ for different centralities.

Centrality	Λ ($\times 10^6$)	$\overline{\Lambda}$ ($\times 10^6$)
0–10%	312.6	296.4
10–30%	49.7	47.2
30–50%	41.2	35.9
50–90%	4.2	3.6

3.4 Efficiency and secondary Λ corrections

The raw L_{proper} spectrum of Λ ($\overline{\Lambda}$) is corrected for the reconstruction efficiency, the feed-down contribution from higher-mass baryons and secondary Λ ($\overline{\Lambda}$) originating from interactions of particles with the detector material as

$$\left[\frac{\mathrm{d}N_\Lambda}{\mathrm{d}L_{\text{proper}}}\right]_{\text{corr}} = \frac{1}{\varepsilon(L_{\text{proper}})} \times f_{\text{prim}}(L_{\text{proper}}) \times \left[\frac{\mathrm{d}N_\Lambda}{\mathrm{d}L_{\text{proper}}}\right]_{\text{raw}}, \tag{2}$$

where $\varepsilon(L_{\text{proper}})$ is the efficiency of primary Λ ($\overline{\Lambda}$) and $f_{\text{prim}}(L_{\text{proper}})$ is the fraction of primary Λ ($\overline{\Lambda}$). The dominant feed-down contributions are given by the weak decays of $\Xi^\pm$, Ξ^0, and $\Omega^\pm$: [1]

- $\Xi^0(\overline{\Xi}^0) \to \Lambda(\overline{\Lambda}) + \pi^0$ BR $= (99.524 \pm 0.012)\%$,
- $\Xi^\pm \to \Lambda + \pi^\pm$ BR $= (99.887 \pm 0.035)\%$,
- $\Omega^\pm \to \Lambda + K^\pm$ BR $= (67.8 \pm 0.7)\%$,
- $\Omega^\pm \to \Xi^0 + \pi^\pm$ and $\Omega^\pm \to \Xi^\pm + \pi^0$ BR $= (32.2 \pm 0.8)\%$.

These corrections are calculated using Monte Carlo (MC) simulations. Collision events between lead ions are simulated using the HIJING event generator [24] and the passage of particles through the experimental apparatus is simulated using GEANT3 [25] as transport code. Considering that the p_{T} distributions of particles and their relative abundances in MC simulations are different from data, centrality and

p_{T}-dependent corrections are applied in MC simulations using weights. These are defined, for different centrality classes, as the ratio of the p_{T} spectrum measured by ALICE and the p_{T} spectrum generated by HIJING.

The ALICE measurements of the p_{T} spectra of Λ, $\Xi^{\pm}$, and $\Omega^{\pm}$ [21, 26] in Pb–Pb collisions at $\sqrt{s_{\mathrm{NN}}} = 2.76$ TeV, scaled by the ratio of the proton p_{T} spectra measured at $\sqrt{s_{\mathrm{NN}}} = 5.02$ TeV [27] and $\sqrt{s_{\mathrm{NN}}} = 2.76$ TeV [28], are used to calculate the weights for different centralities. Based on isospin symmetry, the p_{T} spectra of Ξ^0 are assumed to be identical to those of $\Xi^{\pm}$. Centrality dependent factors, given by the ratios $(\Xi/\Lambda)_{\mathrm{data}}/(\Xi/\Lambda)_{\mathrm{MC}}$ and $(\Omega/\Lambda)_{\mathrm{data}}/(\Omega/\Lambda)_{\mathrm{MC}}$, are also included to reproduce the centrality dependence of the particle ratios observed in data. The efficiency is calculated as the ratio between reconstructed and generated primary Λ in the simulation

$$\varepsilon(L_{\mathrm{proper}}) = \frac{\left[\frac{\mathrm{d}N_{\Lambda}}{\mathrm{d}L_{\mathrm{proper}}}\right]_{\mathrm{rec}}}{\left[\frac{\mathrm{d}N_{\Lambda}}{\mathrm{d}L_{\mathrm{proper}}}\right]_{\mathrm{gen}}}. \tag{3}$$

The efficiencies of Λ and $\overline{\Lambda}$ for central Pb–Pb collisions (0–10%) as a function of L_{proper} are shown in Fig. 2 (left). The correction for secondary Λ ($\overline{\Lambda}$) from material and weak decays is applied by scaling the raw L_{proper} spectrum by the fraction of primary Λ ($\overline{\Lambda}$) given by

$$f_{\mathrm{prim}}(L_{\mathrm{proper}}) = 1 - \frac{\mathrm{d}N_{\Lambda_{\mathrm{sec}}}/\mathrm{d}L_{\mathrm{proper}}}{\mathrm{d}N_{\Lambda_{\mathrm{all}}}/\mathrm{d}L_{\mathrm{proper}}}. \tag{4}$$

The fraction of secondary Λ and $\overline{\Lambda}$ for central Pb–Pb (0–10%) is shown as a function of L_{proper} in the right panel of Fig. 2. The individual contributions from material and weak decays are shown in addition to the total fraction for illustration. The observed trend of the fraction of secondary Λ ($\overline{\Lambda}$) from weak decays with L_{proper} is due to an interplay between the efficiency and decay time of the Λ ($\overline{\Lambda}$) mother particle. For secondary Λ ($\overline{\Lambda}$) from material, it is due to a combined effect of efficiency and the radial distance at which the secondary Λ ($\overline{\Lambda}$) is produced.

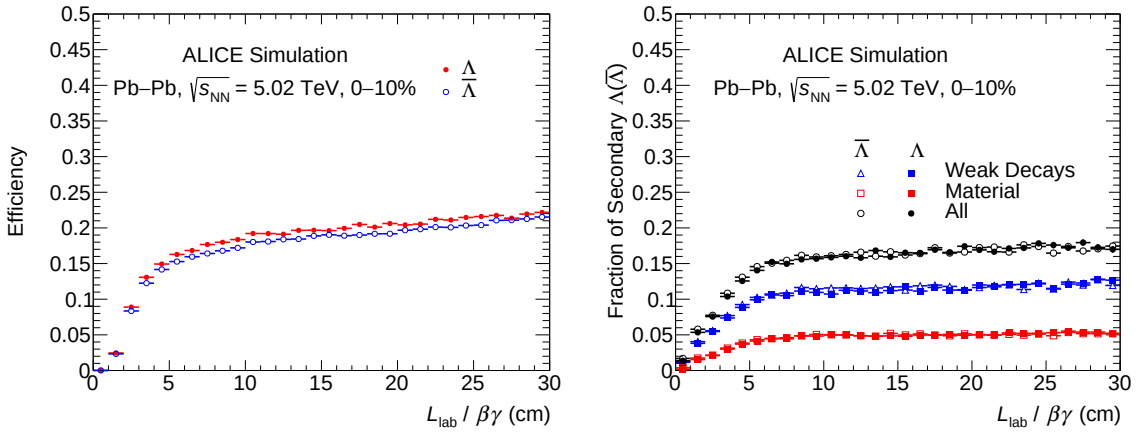

Figure 2: Reconstruction efficiency of primary Λ ($\overline{\Lambda}$) (left) and fraction of secondary Λ ($\overline{\Lambda}$) (right) in central Pb–Pb collisions (0–10%).

4 Systematic uncertainties

The dominant sources of systematic uncertainties on the Λ and $\overline{\Lambda}$ lifetime measurements are related to the track and V^0 selections, signal extraction, efficiency and feed-down corrections. These are summarized

in Table 3. The methods used to estimate the systematic uncertainties from these sources are illustrated in the following. In addition, effects of the material budget uncertainty, the uncertainty on the hadronic interaction of Λ, $\overline{\Lambda}$, and their decay daughters, and potential effects of residual pile-up —which are found to be negligible —are also discussed.

Table 3: Summary of the systematic uncertainties on the Λ and $\overline{\Lambda}$ lifetime measurements. All values are in ps.

Source	Λ	$\overline{\Lambda}$	$\Lambda+\overline{\Lambda}$
Track and V^0 selections	0.55	0.69	0.65
Signal extraction	0.03	0.03	0.02
Efficiency and feed-down corrections	0.30	0.33	0.30
Total	0.63	0.77	0.72

4.1 Systematic uncertainty from track and V^0 selection

The systematic uncertainty due to the track and V^0 selection criteria is estimated by repeating the full analysis chain using one hundred different analysis parameters, where the single-track, topological, and particle-identification selection criteria are varied, such that they produce a maximum variation of $\pm 10\%$ in the raw signal yield, similarly to the approach used in Refs. [21–23]. The systematic uncertainty from the track and V^0 selection is calculated by fitting the distribution of lifetime values obtained from different selection criteria using a Gaussian function and taking the σ of the Gaussian fit as an uncertainty. The obtained uncertainties are 0.55 ps for τ_{Λ}, 0.69 ps for $\tau_{\overline{\Lambda}}$, and 0.65 ps for $\tau_{\Lambda+\overline{\Lambda}}$. This contribution is the dominant source of systematic uncertainty.

4.2 Signal extraction uncertainty

The systematic uncertainty from the signal extraction includes two contributions: the choice of the background fit range and the integration range used for the raw yield extraction. For both contributions, one hundred different intervals are randomly generated, with a uniform probability distribution between two extremes, and the signal extraction procedure is repeated for each of these intervals. The limits used are specified in Table 4.

Table 4: Invariant-mass intervals used for the signal extraction systematic uncertainty.

	Left extreme	Right extreme
Background fit range	$[M_0-14\sigma, M_0-11\sigma]$	$[M_0+20\sigma, M_0+32\sigma]$
Signal integration range	$[M_0-13\sigma, M_0-7\sigma]$	$[M_0+5\sigma, M_0+11\sigma]$

The standard deviation of the distribution of raw yields in each L_{proper} interval is taken as the systematic uncertainty. These two contributions are independent and added in quadrature. The use of alternative fit functions to model the background resulted in negligible changes in the extracted yield. For this reason, this contribution to the signal extraction uncertainty is considered negligible. The uncertainty on the lifetime is calculated by replacing the statistical uncertainties on the corrected L_{proper} spectrum with the signal extraction uncertainties, which are bin-by-bin uncorrelated, and taking the uncertainty from the exponential fit as the systematic uncertainty. This contribution is found to be $(\Delta\tau)^{\text{syst}}_{\text{signal}} = 0.03$ ps for both τ_{Λ} and $\tau_{\overline{\Lambda}}$, and 0.02 ps for $\tau_{\Lambda+\overline{\Lambda}}$.

4.3 Systematic uncertainty from efficiency and feed-down corrections

The systematic uncertainty related to the efficiency and feed-down corrections is estimated by varying: (i) the p_{T}-dependent weights used to adjust the input p_{T} distributions of Λ, Ξ, and Ω in the simulations, (ii)

the Λ, Ξ, and Ω lifetimes by the PDG uncertainties [1] and (iii) the Λ/Ξ and Λ/Ω ratios by the measured uncertainties. The Ω is found to give a negligible contribution to the systematic uncertainties. To vary the lifetimes implemented in the simulations, which are taken from the PDG [1], $L_{\rm proper}$-dependent weights are used. These are obtained as the ratio between the $L_{\rm proper}$ spectrum with modified lifetime and the default spectrum. To estimate the total contribution of these sources, a set of five hundred different efficiency and feed-down corrections is generated. Each of them is obtained using a different set of weights where the $p_{\rm T}$ spectra of Λ, Ξ, and Ω, their lifetimes and particle ratios are varied by a fraction of their uncertainty. Such a fraction is extracted randomly from a Gaussian distribution centered at zero and with a width equal to 1. When modifying the $p_{\rm T}$ spectra measured in data to recalculate the weights, the correlated and uncorrelated uncertainties with $p_{\rm T}$ are treated differently:

1. **$p_{\rm T}$-correlated uncertainties**: all data points of the $p_{\rm T}$ spectrum are shifted coherently upward and downward by a fraction of their systematic uncertainty in each $p_{\rm T}$ interval.
2. **$p_{\rm T}$-uncorrelated uncertainties**: the data points are moved independently by a fraction of their uncorrelated uncertainty in each $p_{\rm T}$ interval.

These five hundred different efficiencies and fractions of secondary Λ ($\overline{\Lambda}$) are then used to correct the raw-$L_{\rm proper}$ spectrum measured in data. The lifetime is extracted for each corrected spectrum and the standard deviation of the distribution of lifetimes is taken as an estimate of the systematic uncertainty from efficiency and feed-down corrections. The obtained uncertainties are 0.30 ps for τ_{Λ}, 0.33 ps for $\tau_{\overline{\Lambda}}$, and 0.30 ps for $\tau_{\Lambda+\overline{\Lambda}}$.

4.4 Inelastic interaction with the detector materials

The default efficiency is based on GEANT3 transport package. The effect of (anti)matter absorption was studied by comparing the default efficiency with that obtained using a MC production based on GEANT4 [29], which contains slightly different parametrizations of the inelastic cross sections of (anti)matter particles. The GEANT3 and GEANT4-based efficiencies are consistent within uncertainties. The Λ and $\overline{\Lambda}$ lifetimes are found to be consistent within uncertainties, and therefore, no systematic uncertainty is assigned due to this effect.

4.5 Material budget

The ALICE detector material is known with a precision of 4.5% [10]. The effect of the limited knowledge of the material budget, which could affect the efficiency and the fraction of secondary Λ ($\overline{\Lambda}$) from material and its dependence on $L_{\rm proper}$, is studied by comparing the efficiency and corrections for secondary Λ ($\overline{\Lambda}$) using MC productions with increased and decreased material density by 4.5%. The difference in the mean lifetime is found to not be statistically significant and therefore this contribution is neglected.

4.6 Pile-up effects

Simultaneous collisions with displaced vertices (pile-up) could, in principle, create a bias in the measurement of the Λ ($\overline{\Lambda}$) decay length due to the wrong V^0–vertex association. The tight selection on the $\cos(\theta_{\rm p})$ allows the matching between a reconstructed V^0 and the wrong vertex only for close vertices. This happens with very low probability and is found to give a negligible bias in the decay length measurement. To further cross-check potential pile-up effects, the analysis is repeated removing all pile-up rejections. The Λ ($\overline{\Lambda}$) lifetimes, in this case, are found to be consistent with the value using default pile-up rejection within the statistical uncertainties. It is concluded that the pile-up effects combined with rather strong topological selections used in this analysis give a negligible effect on the Λ ($\overline{\Lambda}$) lifetime.

5 Results

The L_{proper} spectra of Λ and $\overline{\Lambda}$ measured in each centrality interval are corrected for the corresponding efficiency, feed-down from higher mass baryons, and the fraction of secondary Λ ($\overline{\Lambda}$) from the material. The use of centrality triggers in the data used in this analysis leads to a non-uniform centrality distribution. In order to restore the correct relative contribution from different centralities, the L_{proper} spectra measured in the centrality intervals 10–30%, 30–50%, and 50–90% are scaled by a factor

$$k_i = \frac{N_{\text{events}}^{0-10\%}/w_{0-10\%}}{N_{\text{events}}^{i}/w_i} w_i, \tag{5}$$

where N_{events}^{i} and w_i are the number of events and the centrality bin width of the i-th centrality interval and $N_{\text{events}}^{0-10\%}$ and $w_{0-10\%} = 10$ are those related to the reference centrality interval 0–10%. The obtained spectrum is normalized to unity and fitted with an exponential function in the L_{proper} interval [3,30] cm to extract the mean lifetime. The fit result is shown in Fig. 3, which also contains the data-to-fit ratio in the bottom panel. The data-to-fit ratio in each interval is obtained as the ratio between the interval content and the weighted average of the fit function within the interval, with weight given by the exponential function. In this figure, only statistical uncertainties in each L_{proper} interval and on the mean lifetime are shown. The systematic uncertainties are calculated using the procedure described in Sec. 4 and are reported only for the final result of the lifetime in the 0–90% centrality class. The fit is stable when changing fit range ($L_{\text{proper}}^{\text{min}} = 1,2,3,4,5,...,10$ cm) and binning (width = 0.5,1,2 cm) leading to results that are consistent within the statistical uncertainties.

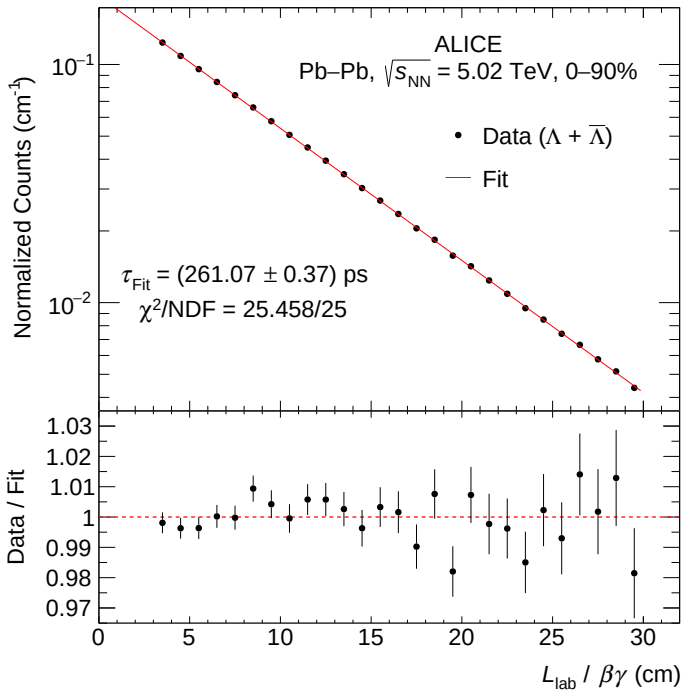

Figure 3: L_{proper} spectrum of Λ and $\overline{\Lambda}$ and exponential fit for the lifetime extraction. Only statistical uncertainties are shown for each data point and for the mean lifetime extracted from the exponential fit.

The measured lifetimes of Λ and $\overline{\Lambda}$ with statistical and systematic uncertainties, are

$$\tau_{\Lambda} = [261.20 \pm 0.49(\text{stat.}) \pm 0.63(\text{syst.})] \text{ ps},$$

$$\tau_{\overline{\Lambda}} = [260.86 \pm 0.55(\text{stat.}) \pm 0.77(\text{syst.})] \text{ ps},$$
$$\tau_{\Lambda+\overline{\Lambda}} = [261.07 \pm 0.37(\text{stat.}) \pm 0.72(\text{syst.})] \text{ ps}.$$

The lifetimes extracted in different centrality intervals are consistent within their statistical uncertainties, as shown in Fig. 4. As a cross-check, the lifetime is also calculated as the weighted average of the results in different centrality intervals, with weights given by the inverse of the statistical uncertainties squared. The result is fully consistent with that extracted from the L_{proper} distribution obtained using Eq. 5.

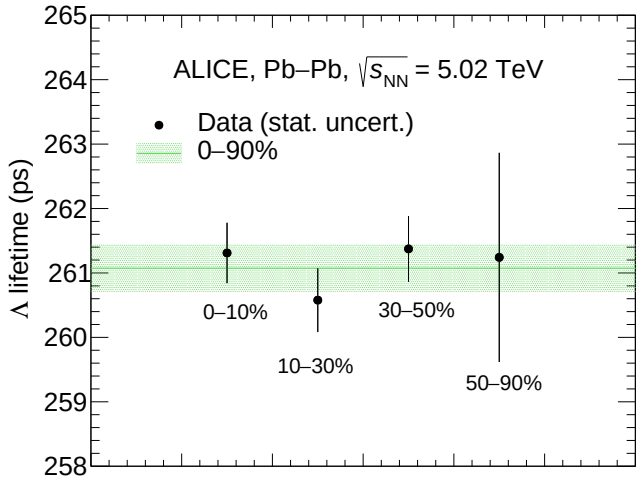

Figure 4: Λ lifetime measured in different centrality intervals. Only statistical uncertainties are shown.

The present measurement is compared with previous results in Fig. 5. The STAR measurement is taken from Ref. [30]. For this comparison, statistical and systematic uncertainties are added in quadrature.

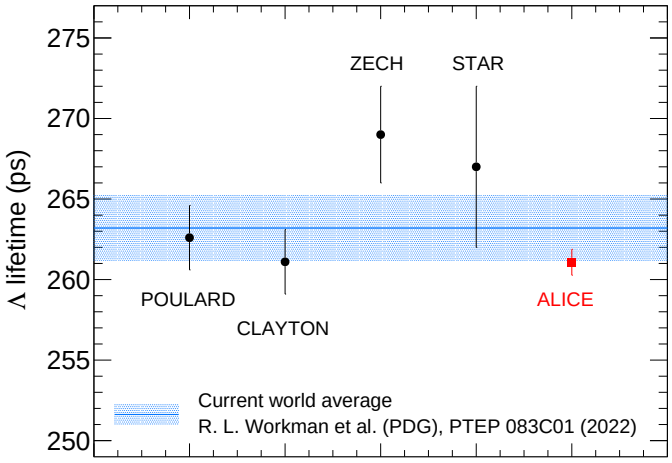

Figure 5: ALICE measurement of the Λ lifetime in comparison with previous measurements [2–4, 30] and the current world average taken from the PDG [1]. Statistical and systematic uncertainties are added in quadrature.

Assuming CPT invariance, the lifetimes of the Λ and $\overline{\Lambda}$ are expected to be consistent within uncertainties. To test CPT invariance, the relative difference $(\tau_{\Lambda} - \tau_{\overline{\Lambda}})/\tau_{\Lambda}$ is measured. Statistical uncertainties on

τ_Λ and $\tau_{\overline{\Lambda}}$ and the systematic uncertainties originating from the signal extraction are uncorrelated and propagated independently. On the other hand, the systematic uncertainties on the efficiency and feed-down corrections as well as those on the track and V^0 selections of Λ and $\overline{\Lambda}$ are partially correlated. The systematic uncertainty on the relative difference $(\tau_\Lambda - \tau_{\overline{\Lambda}})/\tau_\Lambda$ from the former contribution is considered as half of the interval with the following extremes

$$\left[\frac{\tau_{\overline{\Lambda}}}{\tau_\Lambda}\right]_{\text{upper}} = \frac{\tau_{\overline{\Lambda}} + \Delta\tau_{\overline{\Lambda}}(\text{corrections})}{\tau_\Lambda + \Delta\tau_\Lambda(\text{corrections})}, \tag{6}$$

$$\left[\frac{\tau_{\overline{\Lambda}}}{\tau_\Lambda}\right]_{\text{lower}} = \frac{\tau_{\overline{\Lambda}} - \Delta\tau_{\overline{\Lambda}}(\text{corrections})}{\tau_\Lambda - \Delta\tau_\Lambda(\text{corrections})}, \tag{7}$$

and is found to be 1.1×10^{-4}. To take into account the correlation between the uncertainties from the track and V^0 selections, the relative difference $(\tau_\Lambda - \tau_{\overline{\Lambda}})/\tau_\Lambda$ is calculated for each of the different analysis settings used. The uncertainty is given by the standard deviation of the distribution of $(\tau_\Lambda - \tau_{\overline{\Lambda}})/\tau_\Lambda$ values and is found to be 0.0021, which is the largest contribution to the total systematic uncertainty. The measured value of the relative difference $(\tau_\Lambda - \tau_{\overline{\Lambda}})/\tau_\Lambda$ with statistical and systematic uncertainties is

$$(\tau_\Lambda - \tau_{\overline{\Lambda}})/\tau_\Lambda = 0.0013 \pm 0.0028(\text{stat.}) \pm 0.0021(\text{syst.}). \tag{8}$$

This result is shown in Fig. 6 with statistical and systematic uncertainties added in quadrature in comparison with the current value taken from the PDG [1]. The relative difference between the Λ and $\overline{\Lambda}$ lifetimes reported in the PDG is $(\tau_\Lambda - \tau_{\overline{\Lambda}})/\tau_\Lambda = -0.001 \pm 0.009$ [1]. The present measurement is consistent with zero with an overall improvement of the absolute precision with respect to the PDG by approximately a factor of three.

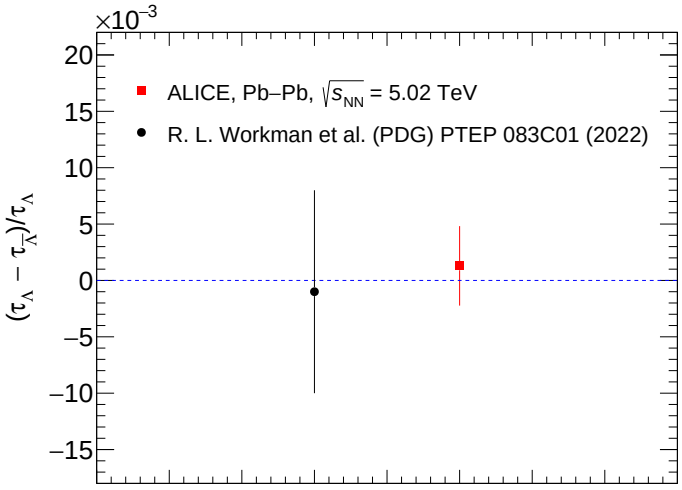

Figure 6: Asymmetry parameter $(\tau_\Lambda - \tau_{\overline{\Lambda}})/\tau_\Lambda$ in comparison with the PDG value [1]. Statistical and systematic uncertainties are added in quadrature.

6 Summary

Unprecedentedly precise measurements of the Λ ($\overline{\Lambda}$) lifetime and of the relative difference between the lifetimes of Λ and $\overline{\Lambda}$ are presented. The latter represents an important test of the CPT symmetry in the strangeness sector. The confidence range of the Λ ($\overline{\Lambda}$) lifetime is reduced by approximately a factor of three with respect to the PDG average.

References

[1] **Particle Data Group** Collaboration, R. L. Workman *et al.*, "Review of Particle Physics", *Prog. Theor. Exp. Phys.* **2022** (2022) 083C01.

[2] G. Poulard, A. Givernaud, and A. Borg, "New measurement of the Λ lifetime", *Phys. Lett. B* **46** (1973) 135–137.

[3] E. F. Clayton *et al.*, "High-statistics determination of the Λ mean lifetime", *Nucl. Phys. B* **95** (1975) 130–134.

[4] G. Zech *et al.*, "A Measurement of the Lifetimes of Ξ^0 and Λ Hyperons", *Nucl. Phys. B* **124** (1977) 413–425.

[5] J. Badier *et al.*, "Reactions pp $\rightarrow \Lambda\Lambda$ at 2.5 GeV/c", *Phys. Lett. B* **25** (1967) 152–155.

[6] P. D. Barnes *et al.*, "Observables in high statistics measurements of the reaction $\overline{\mathrm{p}}\mathrm{p} \rightarrow \overline{\Lambda}\Lambda$", *Phys. Rev. C* **54** (Oct, 1996) 1877–1886.

[7] **ALICE** Collaboration, "Measurement of the lifetime and Λ separation energy of $^{3}_{\Lambda}$H",. https://arxiv.org/abs/2209.07360.

[8] **ALICE** Collaboration, "The ALICE experiment – A journey through QCD", arXiv:2211.04384 [nucl-ex].

[9] **ALICE** Collaboration, K. Aamodt *et al.*, "The ALICE experiment at the CERN LHC", *JINST* **3** (2008) S08002.

[10] **ALICE** Collaboration, B. Abelev *et al.*, "Performance of the ALICE Experiment at the CERN LHC", *Int. J. Mod. Phys.* **A29** (2014) 1430044, arXiv:1402.4476 [nucl-ex].

[11] **ALICE** Collaboration, K. Aamodt *et al.*, "Alignment of the ALICE Inner Tracking System with cosmic-ray tracks", *JINST* **5** (2010) P03003, arXiv:1001.0502 [physics.ins-det].

[12] J. Alme *et al.*, "The ALICE TPC, a large 3-dimensional tracking device with fast readout for ultra-high multiplicity events", *Nucl. Instrum. Meth.* **A622** (2010) 316–367, arXiv:1001.1950 [physics.ins-det].

[13] **ALICE** Collaboration, S. Acharya *et al.*, "Transverse momentum spectra and nuclear modification factors of charged particles in pp, p – Pb and Pb – Pb collisions at the LHC", *JHEP* **11** (2018) 013, arXiv:1802.09145 [nucl-ex].

[14] A. Akindinov *et al.*, "Performance of the ALICE Time-Of-Flight detector at the LHC", *Eur. Phys. J. Plus* **128** (2013) 44.

[15] **ALICE** Collaboration, J. Adam *et al.*, "Determination of the event collision time with the ALICE detector at the LHC", *Eur. Phys. J. Plus* **132** (2017) 99, arXiv:1610.03055 [physics.ins-det].

[16] **ALICE** Collaboration, E. Abbas *et al.*, "Performance of the ALICE VZERO system", *JINST* **8** (2013) P10016, arXiv:1306.3130 [nucl-ex].

[17] **ALICE** Collaboration, B. Abelev *et al.*, "Centrality determination of Pb – Pb collisions at $\sqrt{s_{\rm NN}} = 2.76$ TeV with ALICE", *Phys. Rev.* **C88** (2013) 044909, arXiv:1301.4361 [nucl-ex].

[18] **ALICE** Collaboration, S. Acharya *et al.*, "Centrality determination in heavy ion collisions", ALICE-PUBLIC-2018-011 (2018) . https://cds.cern.ch/record/2636623.

[19] **ALICE** Collaboration, S. Acharya *et al.*, "J/ψ elliptic and triangular flow in Pb – Pb collisions at $\sqrt{s_{\rm NN}} = 5.02$ TeV", *JHEP* **10** (2020) 141, arXiv:2005.14518 [nucl-ex].

[20] **ALICE** Collaboration, K. Aamodt *et al.*, "Strange particle production in proton-proton collisions at $\sqrt{s} = 0.9$ TeV with ALICE at the LHC", *Eur. Phys. J. C* **71** (2011) 1594, arXiv:1012.3257 [hep-ex].

[21] **ALICE** Collaboration, B. Abelev *et al.*, "$\rm K^0_S$ and Λ production in Pb – Pb collisions at $\sqrt{s_{\rm NN}} = 2.76$ TeV", *Phys. Rev. Lett.* **111** (2013) 222301, arXiv:1307.5530 [nucl-ex].

[22] **ALICE** Collaboration, S. Acharya *et al.*, "Multiplicity dependence of (multi-)strange hadron production in proton-proton collisions at $\sqrt{s}$ = 13 TeV", *Eur. Phys. J. C* **80** (2020) 167, arXiv:1908.01861 [nucl-ex].

[23] **ALICE** Collaboration, J. Adam *et al.*, "Enhanced production of multi-strange hadrons in high-multiplicity proton-proton collisions", *Nature Phys.* **13** (2017) 535–539, arXiv:1606.07424 [nucl-ex].

[24] X.-N. Wang and M. Gyulassy, "HIJING: A monte carlo model for multiple jet production in pp, pA, and AA collisions", *Phys. Rev. D* **44** (1991) 3501–3516.

[25] R. Brunand *et al.*, "GEANT Detector Description and Simulation Tool, Program Library Long Write-up",. https://doi.org/10.17181/CERN.MUHF.DMJ1.

[26] **ALICE** Collaboration, B. Abelev *et al.*, "Multi-strange baryon production at mid-rapidity in Pb – Pb collisions at $\sqrt{s_{\rm NN}} = 2.76$ TeV", *Phys. Lett. B* **728** (2014) 216–227, arXiv:1307.5543 [nucl-ex]. [Erratum: Phys.Lett.B 734, 409–410 (2014)].

[27] **ALICE** Collaboration, S. Acharya *et al.*, "Production of charged pions, kaons, and (anti-)protons in Pb – Pb and inelastic pp collisions at $\sqrt{s_{NN}} = 5.02$ TeV", *Phys. Rev. C* **101** (2020) 044907, arXiv:1910.07678 [nucl-ex].

[28] **ALICE** Collaboration, B. Abelev *et al.*, "Centrality dependence of π, k, and p production in Pb – Pb collisions at $\sqrt{s_{NN}} = 2.76$ TeV", *Phys. Rev. C* **88** (2013) 044910, arXiv:1303.0737 [hep-ex].

[29] S. Agostinelli *et al.*, "GEANT4 – a simulation toolkit", *Nucl. Instrum. Meth. A* **506** (2003) 250–303.

[30] **STAR** Collaboration, B. I. Abelev *et al.*, "Observation of an Antimatter Hypernucleus", *Science* **328** (2010) 58–62, arXiv:1003.2030 [nucl-ex].